Multi-parametric 3D Quantitative Ultrasound Vibro-Elastography Imaging for Detecting Palpable Prostate Tumors

Omid Mohareri[1], Angelica Ruszkowski[1], Julio Lobo[1], Joseph Ischia[2], Ali Baghani[3], Guy Nir[1], Hani Eskandari[1,3], Edward Jones[4], Ladan Fazli[4], Larry Goldenberg[2], Mehdi Moradi[1], and Septimiu Salcudean[1]

[1] Department of Electrical and Computer Engineering, University of British Columbia, Vancouver, BC, Canada
[2] Department of Urological Sciences, University of British Columbia, Vancouver, BC, Canada
[3] Ultrasonix Medical Corporation, Richmond, BC, Canada
[4] Department of Pathology and Laboratory Medicine, University of British Columbia, Vancouver, BC, Canada
{tims,omidm,moradi}@ece.ubc.ca

Abstract. In this article, we describe a system for detecting dominant prostate tumors, based on a combination of features extracted from a novel multi-parametric quantitative ultrasound elastography technique. The performance of the system was validated on a data-set acquired from $n = 10$ patients undergoing radical prostatectomy. Multi-frequency steady-state mechanical excitations were applied to each patient's prostate through the perineum and prostate tissue displacements were captured by a transrectal ultrasound system. 3D volumetric data including absolute value of tissue elasticity, strain and frequency-response were computed for each patient. Based on the combination of all extracted features, a random forest classification algorithm was used to separate cancerous regions from normal tissue, and to compute a measure of cancer probability. Registered whole mount histopathology images of the excised prostate gland were used as a ground truth of cancer distribution for classifier training. An area under receiver operating characteristic curve of 0.82 ± 0.01 was achieved in a leave-one-patient-out cross validation. Our results show the potential of multi-parametric quantitative elastography for prostate cancer detection for the first time in a clinical setting, and justify further studies to establish whether the approach can have clinical use.

1 Introduction

Prostate cancer is the most commonly diagnosed cancer among North American men. Even though trans-rectal ultrasound (TRUS) is used to guide prostate interventions because it can image the prostate, standard TRUS imaging is incapable of making a reliable differentiation between malignant and benign tissue

P. Golland et al. (Eds.): MICCAI 2014, Part I, LNCS 8673, pp. 561–568, 2014.

in the gland. Hence, its use is essentially limited to gland volume measurement and procedure guidance. An ideal imaging technique should accurately locate cancer foci in order to guide biopsies and focal therapy.

The use of tissue elasticity as a contrast mechanism to detect prostate tumors has been suggested in many previous studies, in the area of elastography imaging [1–4]. However, most clinical ultrasound elastography systems are based on a quasi-static tissue excitation, with major drawbacks such as dependency on operator skill and lack of reproducibility [5]. Hence, an absolute, quantitative elastography technique is highly desirable. Furthermore, the majority of tested real-time elastography systems are shown to have a high rate of false-positives [2, 6]. One major reason for this poor detection performance is hypothesized to be the fact that the current clinical elastography systems are only capable of producing an image that visualizes a single tissue physical parameter, such as stiffness or compliance, while cancerous tissues are complex and non-uniform and cannot be characterized using only one parameter.

Multi-parametric imaging is an emerging technology that combines information from different techniques, to improve detection rates beyond what can be achieved using any single imaging method. Brock *et al.* assessed a combination approach of ultrasound elastography and contrast enhanced ultrasound and showed that the multi-parametric approach decreased the false-positive value of real-time elastography alone from 34.9% to 10.3% [6]. Vibro-elastography - the multi-frequency tissue response over a wide excitation bandwidth [1, 7], as well as tissue nonlinear response as a function of applied displacements [3], are also shown to contain additional information that may increase the accuracy of cancer detection based on elastography.

In this article, *in vivo* 3D volumetric data acquired from multi-frequency quantitative vibro-elastography imaging is analyzed. This is the first report of such clinical data. We propose a novel set of features that combine the B-mode, strain, absolute elasticity, along with the frequency-dependent parameters that reveal tissue relaxation time and visco-elastic properties. A supervised classification framework is constructed and used to combine the multi-parametric features to separate cancerous and normal tissue and compute a cancer probability map.

2 Methods

Absolute Vibro-Elastography: A multi-frequency steady-state mechanical excitation is applied externally to generate tissue motion. A sequence of n_f frames of RF-data is acquired for each plane in an imaging volume by the ultrasound machine, and processed using a speckle tracking algorithm [8] to create a series of displacements per pixel as a function of time. With a linearity assumption, motion at each pixel has the same temporal frequency content as the input excitation, and therefore the tissue response can be described using complex exponentials (phasor: $p_i = A_i exp(j\phi_i)$) at each pixel for each frequency f_i. A single phasor displacement image is generated from n_f frames for each plane at each frequency and any traveling wave inside the tissue could be revealed from

this image at each plane. Tissue strain could also be computed from this phasor image. The waves seen in phasor displacement images are only 2D projections of the actual traveling waves created by the steady state external excitations. Therefore, 2D phasor images are computed for a series of n_e planes creating a 3D volume. The Local Frequency Estimation (LFE) inversion algorithm [9] was used here for elasticity computation. This process is repeated for an entire volume producing N_E elastograms from N_p planes ($N_E = N_p - n_e + 1$).

System Implementation for Prostate Imaging: The main components of our prostate imaging system are depicted in Figure 1. A BK ultrasound machine (BK Medical, Herlev, Denmark) with a 8848 4-12 MHz biplane transducer was used for imaging the prostate and tissue displacement measurements. Raw In-phase Quadrature (IQ) data was captured at 42.66 Hz sampling rate and saved into an external PC through a DALSA Xcelera-CL PX4 Full frame grabber card (Teledyne DALSA, Waterloo, ON). A previously designed TRUS robot [10] was used to automatically control the rotation angle of the TRUS transducer and save location information of each image.

To ensure good wave penetration into the prostate in a noninvasive manner, we used transperineal excitation similar to the approach used in Magnetic Resonance elastography (MRE) [11]. An electromagnetic exciter in combination with an Agilent U2761A function generator (Agilent Technologies, Santa Clara, CA) was used to generate desired excitation frequencies. The excitation frequencies used for tissue motion generation in this study varied between 58 Hz to 180 Hz. Since we did not have external access to the image acquisition parameters of

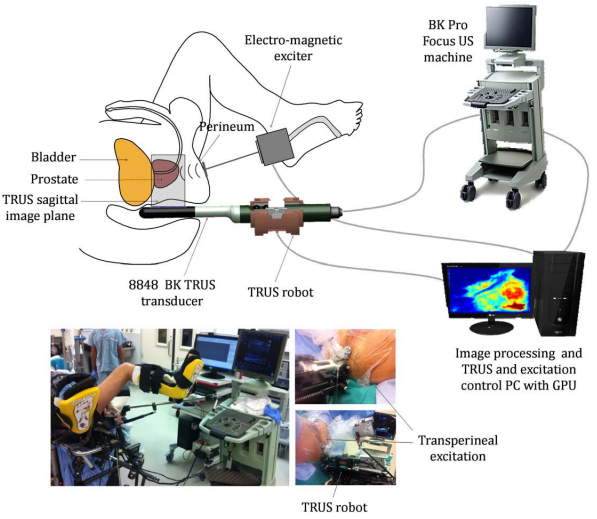

Fig. 1. Main components of the quantitative elastography imaging system with transperineal excitations and the data acquisition system in the clinical setting

the BK ultrasound machine, a band-pass sampling algorithm described in [12] was used here for phase and amplitude reconstruction with sampling frequencies that are lower than the excitation frequencies.

Patient Data Collection: Ten patients with clinically organ-confined prostate cancer (median patient age: 61 years, range: 52-70 and median baseline PSA: 6.4 ng/ml, range: 4.6-36.4) undergoing robotic radical prostatectomy at our institution agreed to participate in this study. For each patient, four to six volumes of multi-parametric data including time displacements, phasor displacement and elasticity data were acquired, for a variety of excitation frequencies. One of the acquired volumes for all patients was at an excitation frequency of 75 Hz and single frequency features were extracted from it. Data from other frequencies were used to compute frequency dependent parameters.

Whole-mount histopathology images of the excised prostate were used as ground truth for cancer detection validation. Each pathology slice was processed by a pathologist who marked the gland boundary, cancer regions and prostate anatomical zone boundaries. Approximately 75% of the cancer occurs in the peripheral zone (PZ). This zone was also segmented on the histopathology slides. Figure 2(a) shows an example pathology slide, and its corresponding acquired B-mode and absolute elastography image from one patient.

2.1 Data Analysis

Feature Extraction: To define regions of interests (ROI) for the classifier data, the acquired images were registered to the pathology images. A slice-to-surface, particle-filter-based registration technique [13] was used to register the

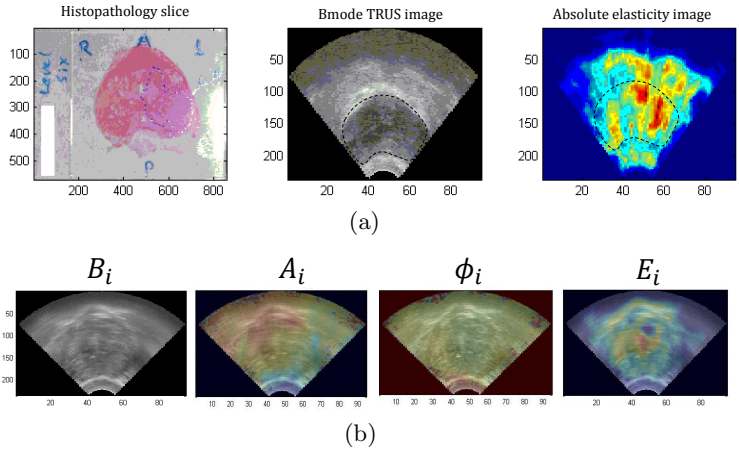

Fig. 2. (a) Example pathology images, and their corresponding reconstructed B-Mode and absolute elastography, (b) example slices of four types of volumetric images available for feature extraction: B-mode (B_i), displacement phasor magnitude (A_i) and phase (ϕ_i), and absolute elasticity (E_i). ($f_i = 75Hz$)

Table 1. Table of features

Data type	Featues per ROI							Index	Meaning
B_i	μ_B	σ_B	Max_B	Min_B	Med_B	$Kurt_B$	$Skew_B$	1-7	Brightness
E_i	μ_E	σ_E	Max_E	Min_E	Med_E	$Kurt_E$	$Skew_E$	8-14	Stiffness
A_i	μ_A	σ_A	Max_A	Min_A	Med_A	$Kurt_A$	$Skew_A$	15-21	Strain
ϕ_i	μ_ϕ	σ_ϕ	Max_ϕ	Min_ϕ	Med_ϕ	$Kurt_\phi$	$Skew_\phi$	22-28	
Frequency-response	m_ϕ							29	Relaxation-time
	m_E							30	Viscosity

stack of equispaced 2D pathology contours to the 3D surface extracted from the volumetric ultrasound images.

For each plane in each volume, four types of images are available for feature extraction: B-mode (B_i), displacement phasor magnitude (A_i) and phase (ϕ_i), and absolute elasticity (E_i). To identify ROIs, regions of interest were specified for both Class 1 (malignant cancer) and Class 0 (benign lesion) using the pathology markings which were registered to ultrasound data. A feature vector was created for each ROI corresponding to a whole tumor or a non-cancerous area. For each of the four data types (B_i, A_i, ϕ_i, E_i), seven statistical parameters of the pixel intensities within the ROI were calculated and used as features. These included the mean, standard deviation, maximum, minimum, median, kurtosis and skewness. Before extracting the features, histogram normalization was performed on the data across the data-set to map the intensities to the same dynamic rage for all cases. A feature vector with $n = 28$ components (described in Table 1) was created per ROI, all calculated from images with excitation at 75 Hz.

In order to leverage the multi-frequency data for each patient, two frequency dependent features were computed for each ROI and added to the feature vector. The displacement phasor phase (ϕ_i) and elasticity (E_i) frequency-response were analyzed for the range of frequencies available for each patient.

Assuming linearity, the tissue displacement transfer function could be formulated as: $G(j\omega) \cong \frac{X(j\omega)}{U(j\omega)} = \frac{1}{1+Tj\omega}$, where $X(j\omega)$ is the displacement measured at each pixel, $U(j\omega)$ is the input displacement from external excitation, and T is a time-constant. The phase of this transfer function is $\angle G(j\omega)$=arctan($T\omega$), which is the same as the computed phasor phase ϕ_i at each frequency. Hence, the slope of a line fitted to the ϕ_i frequency-response will be T, an estimate of the tissue relaxation time. Such analysis was performed for each ROI in our data-set, and the slope of a line fitted to the ϕ_i frequency response was computed (m_ϕ) and added to the feature vector.

Tissue visco-elastic properties are reported to vary with the input excitation frequency [1] and the rate of such variations may yield more information about tissue characteristics. The frequency response of E_i was computed for each ROI and the slope of a line fitted to the curve (m_E), rate of change of elasticity with frequency, was included as another feature for each ROI. Using the combination of all described features, we incorporated the texture and intensity features from one common frequency and also used the multi-frequency content of the data.

Classification: Binary classification between malignant and benign lesions was performed using random forests [14] with bootstrapping of features and Gini Index. The following forest parameters were optimized using a grid-search method with a leave-one-patient-out cross-validation: (i) number of estimators/trees (N_e), (ii) maximum number of features considered when finding the best binary split (Max_{nf}), (iii) maximum depth of the tree (Max_{nt}).

To perform classifications consistent with the tissue types in the prostate gland, features were extracted twice: (i) only from the peripheral zone (PZ) of the prostate, (ii) from the whole gland (WG), since different regions in the prostate have inherently different elastic properties [15].

In order to demonstrate the performance of each group of features, four classification experiments with different feature vectors were performed: (i) multi-parametric and multi-frequency experiment ($n = 30$, feature index: 1-30 in Table 1), (ii) multi-parametric single-frequency experiment ($n = 28$, feature index: 1-28), (iii) multi-parametric and multi-frequency experiment without B-Mode features ($n = 23$, feature index: 8-30), (iv) single-frequency single-parametric experiment ($n = 7$, feature index: 8-14).

3 Results

The classification results in terms of sensitivity, specificity, accuracy and area under the ROC curve (AUC) for each experiments are presented in Table 2. In plotting the receiver operating characteristic (ROC) curve, a value of probability=0.5 was used as the cutoff between classes.

Comparison of Results in Each Prostate Region: For each of the experiments with different feature groups, the classification algorithms were tested once on ROIs extracted from the PZ, and once on ROIs from the WG. Results suggest that limiting the analysis to the PZ would consistently lead to better results in terms of AUC, specificity and accuracy (AUC changes from 0.79 ± 0.01 to 0.82 ± 0.01 in experiment (i)).

Comparison of Results for Different Feature Groups: Comparing the results of the multi-frequency multi-parametric experiment with single-frequency single-parameter elasticity imaging shows $\approx$ 10% improvement in AUC and specificity in the PZ. Single-frequency single-parameter experiments represent the traditional single parameter elasticity imaging. Comparison between the results of experiment (i) and (ii) shows 4% improvement in an AUC and 7% improvement in the specificity in the PZ, when multi-frequency features are added to the feature vector. Without using features from B-Mode, the multi-frequency multi-parametric elasticity imaging could yield an AUC of 0.77 (compare the results of experiments (i), (iii)).

Table 2. Classification results. n: number of features, f-index: feature index, Zone: prostate region features extracted from, N_{ROI}: number of ROIs extracted, Param.: [N_e, Max_{nf}, Max_{nt}] for random forest, AUC: area under ROC curve. Results corresponding to PZ are colored in gray for easier comparison.

Random forest classification results									
Ex	n	f-index	Zone	N_{ROI}	Param.	Accuracy	Sensitivity	Specificity	AUC
i	30	1-30	PZ	164	[19, 19, 2]	0.72±0.01	0.61±0.02	0.82±0.04	0.82±0.01
			WG	231	[18, 14, 2]	0.67±0.01	0.63±0.03	0.74±0.02	0.79±0.01
ii	28	1-28	PZ	164	[17, 18, 2]	0.69±0.02	0.62±0.02	0.75±0.03	0.78±0.01
			WG	231	[17, 19, 2]	0.66±0.01	0.61±0.03	0.72±0.02	0.77±0.01
iii	23	8-30	PZ	164	[16, 17, 2]	0.65±0.02	0.61±0.02	0.72±0.03	0.77±0.01
			WG	231	[13, 4, 7]	0.64±0.02	0.60±0.04	0.68±0.02	0.75±0.02
iv	7	8-14	PZ	164	[19, 2, 2]	0.64±0.01	0.63±0.01	0.69±0.01	0.73±0.02
			WG	231	[18, 3, 2]	0.64±0.02	0.64±0.01	0.63±0.01	0.70±0.02

4 Discussions and Conclusions

Previous reports on the clinical application of elastography for prostate cancer detection all confirm its usefulness, but also agree on the fact that single parametric elasticity imaging alone is not sufficiently accurate to enable guidance for diagnosis and treatment. In the published clinical studies with whole mount histopathology validation, Brock *et al.*, reported an overall sensitivity and specificity of 49% and 73.6% using shear-wave elastography [2]. Salomon *et al.* reported sensitivity and specificity of 75.4% and 76.6%, using quasi-static elastography [16]. We show that the combination of all features (experiment (i)) provides sensitivity of 61% and specificity of 82% and has a more efficient cancer detection performance than each method individually.

Nodular prostatic hyperplasia was observed inside the prostate transition zone for 80% of the cases. It causes changes in the tissue mechanical properties and could contribute to some of the false positive detections outside the PZ. Hence, the elasticity reconstruction is expected to perform better in the PZ region, leading to more accurate results.

Feature importance analysis from random forest classification shows that $Kurt_\phi$, $Kurt_A$, $Kurt_E$ have the highest importance rank in the classification results. Kurtosis is a measure of "peakedness"of the distribution of the parameters in each ROI. Such results reveal that a dominant tumor typically has a consistent intensity contrast with respect to the surrounding healthy tissue in elasticity and displacement phasor images.

A multi-parametric cancer detection framework based on quantitative vibro-elastography imaging was proposed in this paper. A unique set of features were computed based on the acquired data from 10 patients in a feasibility clinical study, and their detection performance was compared with traditional single parameter elastography. Promising detection results justify further clinical studies to prove the clinical usability of the system.

References

1. Salcudean, S.E., Sahebjavaher, R.S., et al.: Biomechanical modeling of the prostate for procedure guidance and simulation. In: Soft Tissue Biomechanical Modeling for Computer Assisted Surgery, vol. 11, pp. 169–198. Springer (2012)
2. Brock, M., Von Bodman, C., et al.: The impact of real-time elastography guiding a systematic prostate biopsy to improve cancer detection rate: A prospective study of 353 patients. J. Urol. 187(6), 2039–2043 (2012)
3. Zhang, M., Nigwekar, P., et al.: Quantitative characterization of viscoelastic properties of human prostate correlated with histology. Ultrasound Med. Biol. 34(7), 1033–1042 (2008)
4. Zhai, L., Madden, J., et al.: Acoustic radiation force impulse imaging of human prostates ex vivo. Ultrasound Med. Biol. 36(4), 576–588 (2010)
5. Ahmad, S., Cao, R., et al.: Transrectal quantitative shear wave elastography in the detection and characterisation of prostate cancer. Surg. Endosc. 27(9), 3280–3287 (2013)
6. Brock, M., Eggert, T., et al.: Multiparametric ultrasound of the prostate: adding contrast enhanced ultrasound to real-time elastography to detect histopathologically confirmed cancer. J. Urol. 189(1), 93–98 (2013)
7. Turgay, E., Salcudean, S., et al.: Identifying mechanical properties of tissue by ultrasound. Ultrasound Med. Biol. 32(2), 221–235 (2008)
8. Zahiri-Azar, R., Salcudean, S.E.: Motion estimation in ultrasound images using time domain cross correlation with prior estimates. IEEE Trans. Biomed. Eng. 53(10), 1990–(2000)
9. Muthupillai, R., Lomas, D.J.: Magnetic resonance elastography by direct visualization of propagating acoustic strain waves. Science 269(5232), 1854–1857 (1995)
10. Adebar, T., Salcudean, S., Mahdavi, S., Moradi, M., Nguan, C., Goldenberg, L.: A robotic system for intra-operative trans-rectal ultrasound and ultrasound elastography in radical prostatectomy. In: Taylor, R.H., Yang, G.-Z. (eds.) IPCAI 2011. LNCS, vol. 6689, pp. 79–89. Springer, Heidelberg (2011)
11. Sahebjavaher, R.S., Baghani, A., et al.: Transperineal prostate mr elastography: Initial in vivo results. Magn. Reson. Med. 69(2), 411–420 (2013)
12. Eskandari, H., Goksel, O., et al.: Bandpass sampling of high-frequency tissue motion. IEEE Trans. Ultrason. Ferroelectr. Freq. Control. 58(7), 1332–1343 (2011)
13. Nir, G., Salcudean, S.E.: Registration of whole-mount histology and tomography of the prostate using particle filtering. In: Proc. SPIE, vol. 8676, pp. 86760E–86760E–9 (2013)
14. Breiman, L.: Random forests. Mach. Learn. 45(1), 5–32 (2001)
15. McNeal, J.E., Redwine, A.E., et al.: Zonal distribution of prostatic adenocarcinoma. correlation with histologic pattern and direction of spread. Am. J. Surg. Pathol. 12(12), 897–906 (1988)
16. Salomon, G., Kollerman, J., et al.: Evaluation of prostate cancer detection with ultrasound real-time elastography: A comparison with step section pathological analysis after radical prostatectomy. Eur. Urol. 54(6), 1354–1362 (2008)